ELSEVIER

Catalysis Today 64 (2001) 309–320

CATALYSIS TODAY

www.elsevier.com/locate/cattod

Catalytic wet air oxidation with a deactivating catalyst analysis of fixed and sparged three-phase reactors

Faïçal Larachi [a,*], Ion Iliuta [b], Khaled Belkacemi [c]

[a] *Department of Chemical Engineering and CERPIC, Université Laval, Ste-Foy, Que., Canada G1K 7P4*
[b] *Department of Chemical Engineering, Faculty of Industrial Chemistry, University Politehnica of Bucharest, Polizu 1, 78126 Bucharest, Romania*
[c] *Department of Food Sciences and Nutrition, Université Laval, Ste-Foy, Que., Canada G1K 7P4*

Abstract

A comparative analysis is made for a trickle-bed reactor, a packed-bubble column, a three-phase fluidized bed and a slurry-bubble column with an active and moderately deactivating catalyst for the wet oxidation at high pressure and temperature of organic-containing aqueous wastes. Compared to other mature industrial sectors where multiphase reactors are prevalent, the design of three-phase catalytic reactors for wet air oxidation processes is still at an emerging stage. This paper discusses, from a multiphase reactor engineering perspective, the design of such contactors by setting an exhaustive modeling framework of catalytic wet oxidation in which the molecular, particle and reactor scales are integrated. The simulation results indicate that when wet oxidation is liquid-reactant limited, packed-bubble columns outperform trickle beds, whereas slurry-bubble columns are the most vulnerable to "coke" deactivation.

Keywords: Heterogeneous wet oxidation; Detoxification; Wastewater; Trickle bed; Packed- and slurry-bubble column; Fluidization; Deactivation

1. Introduction

Water is becoming an increasingly coveted commodity so that regional and planetary policies are being implemented for the safeguard and the parsimonious exploitation of water resources. However, the management of toxic and hazardous wastewaters streams is still a perennial problem. Due to the reinforcement of the regulations for quality control of effluents, the manufacturing industries have to minimize their emissions of organic and inorganic wastes using efficient routes via the so-called "atom economy" concept which consists in maximizing the atom utilization from the raw materials to the final products [1,2]. In addition, it is vital to develop highly efficient processes capable of destroying hazardous xenobiotic pollutants contained in non-compressible waste effluents.

Aqueous wastes having an organic pollutant load in the range of few hundred to few thousand parts per million are too dilute to incinerate, yet too toxic to bio-treat. Such wastes can be suitably dealt with by means of sub-critical (solid-) catalyzed wet oxidation (CWO). The recourse to solid catalysts offers a practical technological alternative to the conventional non-catalytic or homogeneously catalyzed routes [3,4] because not only can the treatment be carried out under much milder conditions, but the catalyst may in principle be easily recovered, regenerated and reused. Laboratory tests reveal that CWO is so

* Corresponding author. Tel.: +1-418-656-3566; fax: +1-418-656-5993.
E-mail address: flarachi@gch.ulaval.ca (F. Larachi).

0920-5861/01/$ – see front matter
PII: S0920-5861(00)00534-4

Nomenclature

a_s	external area of the particles per unit reactor volume (m^{-1})
C_j	concentration of lump j ($kmol/m^3$)
$C^o_{j\ell}$	j-component concentration in feed stream ($kmol/m^3$)
C_s	solids concentration (kg/m^3)
$\bar{C}_s$	average solids concentration (kg/m^3)
d_p	particle diameter (mm, μm)
D^{eff}_j	j-component effective diffusivity (m^2/s)
D_ℓ	liquid axial dispersion coefficient (m^2/s)
D_s	solids axial dispersion (m^2/s)
H	bed height (m)
k, k'	lumped rate constants (mol/kg min)
K, K'	adsorption equilibrium constants ($m^3/kmol$)
$k_{j\ell s}$	j-component liquid–solid mass transfer coefficient (m/s)
$(ka)_{\ell\ell}$	mass transfer coefficient between dynamic and stagnant liquid zones (s^{-1})
r	radial position within catalyst particle (m)
r_j	reaction rate (mol/min kg catalyst)
r_p	radius of catalyst particle (m)
t	time (s)
v_g	gas superficial velocity (m/s)
v_ℓ	liquid superficial velocity (m/s)
$v_{\ell mf}$	minimum liquid fluidization velocity (m/s)
$v_{\ell s}$	superficial slurry velocity (m/s)
v_p	hindered settling velocity (m/s)
X	phenol conversion
z	longitudinal coordinate (m)

Greek letters

α	deactivation function
ε_g	gas holdup
ε_ℓ	liquid holdup
ε_p	particle internal porosity
ε_s	solid holdup
η	effectiveness factor
η_d	dynamic external wetting efficiency, $\eta_d = \eta_e\varphi$
η_e	external wetting efficiency
η_s	static external wetting efficiency, $\eta_s = \eta_e(1-\varphi)$
ρ_s	catalyst particle density (kg/m^3)
φ	fraction of dynamic liquid, $\varphi = \varepsilon^d_\ell/\varepsilon_\ell$
$\bar{\psi}_\ell$	volumetric average liquid fraction in the slurry

Subscripts

A	phenolic carbon, A lump
B	carbon of oxidation intermediates, B lump
C	carbon of fully mineralized products, C lump
d	dynamic
ℓ	liquid
s	solid, static

Superscripts

d	dynamic
s	static
$*$	on catalyst surface
–	average
o	feed

versatile that wastewaters containing a broad spectrum of organic and/or inorganic pollutants including carbon (C), oxygen (O), nitrogen (N), halogen (X), sulfur (S) and phosphorus (P)-bearing molecules are tackled efficiently.

CWO liquid-phase oxidation processes fall into the category of gas–liquid–solid reactions and are still not at a mature stage of development and technological implementation [2]. Their multiphase character poses many chemical reactor engineering and design challenges as the overall outcome of such processes depends in a complex manner on the inter-phase and intra-particle heat and mass transport, kinetics, thermodynamics, flow patterns and hydrodynamics. Despite the myriad of laboratory studies being released in the academic and patent literature, there are too few industrially demonstrated applications of CWO. The Nippon Shokubai LC Process (Japan) using a monolith reactor with a Pt–Pd/TiO_2/ZrO_2 wash-coat, the Osaka Gas and the Kurita processes are the only three known industrial applications to date [5].

References in the open literature on scientific approaches to the design of three-phase reactors for CWO are to our knowledge non-existent. There are

only two studies on computer-aided tools for the design of non-catalytic wet air oxidation bubble column reactors [6,7]. There is an urgent need to bring new knowledge and information from the perspective of multiphase reactor engineering to gas–liquid–solid catalytic wet oxidation. This is the goal of the present contribution which presents an analysis of a catalytic wet oxidation reaction in the presence of catalyst deactivation in four types of multiphase reactors: a trickle-bed reactor, a packed-bubble column, a three-phase fluidized bed and a slurry-bubble column.

2. A case study: wet oxidation of aqueous phenol, a model toxic wastewater

Time and space dependent models are developed to analyze the performance of four common three-phase reactors for catalytic liquid-phase oxidation of phenol aqueous solutions under deactivating conditions. For the four candidate reactors, i.e. cocurrent downflow trickle-bed reactors, cocurrent upflow packed-bubble columns, cocurrent upward gas–liquid fluidized beds, and slurry-bubble columns with through-flow of the catalyst powder, the following general assumptions are made in developing the mathematical models:

- The organics are assumed to be non-volatile and the reaction is taking place solely in the liquid phase.
- The concentration level of pollutant in the feed stream is low, so that the reactors are isothermal.
- Wet oxidation reactions are intrinsically not fast and usually carried out in a large excess of oxygen. The actual concentration of dissolved oxygen is therefore assumed close to equilibrium concentration.
- For reactors with fixed catalysts there is mass transfer between the dynamic and static liquid holdups and intra-particle liquid.
- For the reactors with moving catalysts, there is mass transfer between the external liquid holdup and the intra-particle liquid.
- No correction of effective diffusivity is made to account for the progressive deactivation by the carbonaceous deposit.
- The catalyst is assumed to be internally completely wet.
- Inside the particle the diffusion of reactants occurs in the liquid.
- For downflow fixed-bed reactors, both partial and full wetting of the external surface can occur. For the other three configurations, full external wetting is fulfilled at all times.

2.1. Reaction network

The reaction between phenol and an excess of soluble oxygen proceeds in the presence of a deactivating solid catalyst. The 7/3 MnO_2/CeO_2 composite oxide catalyst considered here undergoes *fouling* deactivation by carbonaceous deposits. Detailed quantitative and qualitative studies of this reaction [8,9] showed that apart from the main reaction where phenol (A) mineralizes into total inorganic carbon (C), a number of side and intermediate reactions are also possible. The complete multiple deactivation-reaction network describing phenol CWO is shown in Fig. 1 in which all the intervening species are grouped into four lumps.

Chemisorbed phenol (lump A) converts into chemisorbed aqueous break-down oxidation intermediate lump (B) that in turn further degrades into oxidation end-product lump C (total inorganic carbon). All three lumped species can instantaneously adsorb or desorb. Concomitant with these steps, a foulant (lump W) is formed by a series of complex polymerization reactions between lumps A and B [10], and irreversibly adsorbs to progressively block the active sites on the catalyst surface.

A Langmuir–Hinshelwood–Hougen–Watson kinetic model based on this deactivation-reaction network has been used to predict the fate of the various carbon lumps as well as the decline of catalyst activity during phenol wet oxidation [8]

$$r_A = \frac{k_2 K_1 \alpha C_{A\ell}}{1 + K_1 C_{A\ell} + K_3 C_{B\ell} + K_3' C_{C\ell}} \quad (1)$$

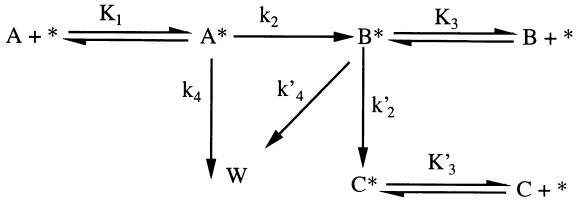

Fig. 1. Deactivation-reaction network for phenol CWO with the formation of carbonaceous foulant [8].

$$r_{\mathrm{B}} = \frac{(k_2 K_1 C_{\mathrm{A}\ell} - k_2' K_3 C_{\mathrm{B}\ell})\alpha}{1 + K_1 C_{\mathrm{A}\ell} + K_3 C_{\mathrm{B}\ell} + K_3' C_{\mathrm{C}\ell}} \tag{2}$$

$$-\frac{\mathrm{d}\alpha}{\mathrm{d}t} = \frac{(k_4 K_1 C_{\mathrm{A}\ell} + k_4' K_3 C_{\mathrm{B}\ell})\alpha}{1 + K_1 C_{\mathrm{A}\ell} + K_3 C_{\mathrm{B}\ell} + K_3' C_{\mathrm{C}\ell}} \tag{3}$$

2.2. Pellet-scale model

Description of the simultaneous transport across, and consumption within, each catalyst particle requires that time and space mapping of phenol and B lump concentrations, as well as the activity loss rate $-\mathrm{d}\alpha/\mathrm{d}t$ be simulated. To accomplish this task and assuming spherical symmetry, the pellet-scale mass balance equations to be solved are

$$\varepsilon_{\mathrm{p}} \frac{\partial C_{j\ell}}{\partial t} = r^{-2} \frac{\partial}{\partial r}\left(r^2 D_j^{\mathrm{eff}} \frac{\partial C_{j\ell}}{\partial r}\right) - \rho_{\mathrm{s}} r_j (C_{\mathrm{A}\ell}, C_{\mathrm{B}\ell}, C_{\mathrm{C}\ell}, \alpha)$$

$$\text{in which } j = \mathrm{A} \text{ or } \mathrm{B} \tag{4}$$

$$-\frac{\partial \alpha}{\partial t} = \frac{(k_4 K_1 C_{\mathrm{A}\ell} + k_4' K_3 C_{\mathrm{B}\ell})\alpha}{1 + K_1 C_{\mathrm{A}\ell} + K_3 C_{\mathrm{B}\ell} + K_3' C_{\mathrm{C}\ell}} \tag{5}$$

The corresponding boundary and initial conditions for these equations are the following:

1. when $r = 0$

$$\frac{\partial C_{j\ell}}{\partial r} = 0 \tag{6}$$

2. no solids mixing (for fluidized bed and slurry-bubble column reactors $\varphi = 1$, $\eta_{\mathrm{e}} = 1$): when $r = r_{\mathrm{p}}$

$$-D_j^{\mathrm{eff}} \left.\frac{\partial C_{j\ell}}{\partial r}\right|_{r=r_{\mathrm{p}}} = k_{j\ell \mathrm{s}}^{\mathrm{d}} \eta_{\mathrm{e}} \varphi (C_{j\ell}^{\mathrm{d}} - C_{j\ell}^{*}) + k_{j\ell \mathrm{s}}^{\mathrm{s}} \eta_{\mathrm{e}} (1-\varphi)(C_{j\ell}^{\mathrm{s}} - C_{j\ell}^{*}) \tag{7}$$

3. complete solids mixing (fluidized bed reactors): when $r = r_{\mathrm{p}}$

$$-a_{\mathrm{s}} H\, D_j^{\mathrm{eff}} \left.\frac{\partial C_{j\ell}}{\partial r}\right|_{r=r_{\mathrm{p}}} = v_\ell (C_{j\ell}^{\mathrm{o}} - C_{j\ell}|_{z=H}) \tag{8}$$

4. when $t = 0$

$$C_{j\ell}(r, 0) = C_{j\ell}^{\mathrm{o}};\ \alpha = 1 \tag{9}$$

2.3. Reactor-scale models

The three-phase reactor models, in which momentum and mass transfer, chemical kinetics and flow patterns are intertwined, are initial value problems. Their equations of change for concentration of the different species are integrated over time, reactor and catalyst pellet lengths.

2.3.1. Fixed-bed reactors

The model for the cocurrent gas–liquid trickle-bed and packed-bubble column is comprised of two unsteady-state mass balance equations written for each of the aqueous A and B lumps. It accounts for:

- the species accumulation, advection and axial dispersion in the dynamic liquid;
- the species accumulation in the static liquid;
- the liquid–liquid mass transfer across the dynamic-static liquid interface;
- the contacting and (dynamic) liquid–solid mass transfer between pellets and dynamic liquid;
- the contacting and (static) liquid–solid mass transfer between pellets and static liquid;
- the partial wetting and distinction between static and dynamic wetting efficiencies.

From a computational standpoint, the piston dispersion exchange (PDE) model is used to capture both transient and space dependence in phenol and B lump concentrations within each of the dynamic and the static liquid zones as follows:

$$\varepsilon_\ell^{\mathrm{d}} \frac{\partial C_{j\ell}^{\mathrm{d}}}{\partial t} + v_\ell \frac{\partial C_{j\ell}^{\mathrm{d}}}{\partial z} = D_\ell \varepsilon_\ell^{\mathrm{d}} \frac{\partial^2 C_{j\ell}^{\mathrm{d}}}{\partial z^2} - (ka)_{\ell\ell}(C_{j\ell}^{\mathrm{d}} - C_{j\ell}^{\mathrm{s}}) - \eta_{\mathrm{d}} k_{j,\ell \mathrm{s}}^{\mathrm{d}} a_{\mathrm{s}} (C_{j\ell}^{\mathrm{d}} - C_{j\ell}^{*}) \tag{10}$$

$$\varepsilon_\ell^{\mathrm{s}} \frac{\partial C_{j\ell}^{\mathrm{s}}}{\partial t} = (ka)_{\ell\ell}(C_{j\ell}^{\mathrm{d}} - C_{j\ell}^{\mathrm{s}}) - \eta_{\mathrm{s}} k_{j,\ell \mathrm{s}}^{\mathrm{s}} a_{\mathrm{s}} (C_{j\ell}^{\mathrm{s}} - C_{j\ell}^{*}) \tag{11}$$

2.3.2. Fluidized bed and slurry-bubble column

For the cocurrent gas–liquid upflow fluidized and slurry-bubble column reactors, static liquid vanishes ($\varepsilon_\ell^{\mathrm{s}} = \eta_{\mathrm{s}} = 0$; $(ka)_{\ell\ell} = 0$; $\eta_{\mathrm{d}} = 1$) and the reactor model becomes

$$\varepsilon_\ell \frac{\partial C_{j\ell}}{\partial t} + v_\ell \frac{\partial C_{j\ell}}{\partial z} = D_\ell \varepsilon_\ell \frac{\partial^2 C_{j\ell}}{\partial z^2} - k_{j,\ell \mathrm{s}} a_{\mathrm{s}} (C_{j\ell} - C_{j\ell}^{*}) \tag{12}$$

In the case of slurry-bubble column, the solids concentration longitudinal distribution is described by a sedimentation–dispersion model [11–13]. The mass balance of solids as a function of the longitudinal coordinate gives

$$\frac{\partial C_s}{\partial t} = \frac{\partial}{\partial z}\left(D_s \frac{\partial C_s}{\partial z}\right) + \frac{\partial}{\partial z}\left(C_s\left(\frac{v_{\ell s}}{1-\varepsilon_g} - \bar{\psi}_\ell v_p\right)\right) \tag{13}$$

The assumption used in deriving Eq. (13) is that the gas holdup and the fraction of liquid in the slurry are independent of the vertical position, i.e. particle density is always much greater than solids concentration. Average volumetric fraction of the liquid in the liquid–solid slurry is expressed as a function of average solids concentration as [12]

$$\bar{\psi}_\ell = 1 - \frac{\bar{C}_s}{\rho_s} \tag{14}$$

2.3.3. Initial and boundary conditions for reactors

The phenol and B intermediate initial concentrations in dynamic, static or total liquid zones are as in the feed stream:

1. when $t = 0$

$$C_{j\ell}^d = C_{j\ell}^s = C_{j\ell}^o \quad \text{for Eqs. (10) and (11)} \tag{15}$$

$$C_{j\ell} = C_{j\ell}^o \quad \text{for Eq. (12)} \tag{16}$$

2. when $z = 0$

$$v_\ell C_{j\ell}^o = v_\ell C_{j\ell}^d|_{z=0^+} - D_\ell \varepsilon_\ell^d \frac{\partial C_{j\ell}^d}{\partial z} \tag{17}$$

when $z = H$

$$\frac{\partial C_{j\ell}^d}{\partial z} = 0 \tag{18}$$

The boundary conditions for the description of the solids concentration distribution in a slurry-bubble column have been a point of controversy for several years [11–13]. Several authors hold that the solids concentration at the top of the column is equal to the effluent or feed concentration, while others considered them different. In this work, the solids concentration at the top of the slurry-bubble column is correlated to the solids inlet concentration using the Smith and Ruether [12] empirical correlation: when $z = H$

$$C_s = 1.27 C_s^o \tag{19}$$

2.4. Operating conditions and thermodynamics

The characteristics of the porous MnO_2/CeO_2 catalyst particles, the design and geometric parameters of the three-phase reactors, the operating conditions and the values of the kinetic parameters are indicated in Table 1.

Water being the overwhelming compound and the phenol concentration being relatively small (100–2800 ppm), the physical properties specific to water are used for the liquid phase. Moreover, because of the moderate severity level of the simulated oxidation (0.5 MPa and 80°C) and dilute water conditions, it is not necessary to use detailed equations of state for the fluid phases. Fugacity and activity coefficients as well as compressibility factor for oxygen and water are all assigned unity values. Raoult's and Henry's laws are assumed to be valid for water and oxygen, respectively.

2.5. Hydrodynamic parameters

Fixed bed reactors. For trickle bed, CWO is run in the trickle flow regime under partial and full wetting conditions of pellets, whereas for the same operating conditions the packed-bubble column operates in the bubble flow regime with fully wetted pellets. The external liquid holdup, ε_ℓ, is calculated using the extended Holub model [14] for trickle beds, and using the neural network correlation of Bensetiti et al. [15] for the packed-bubble column. The static liquid holdup, ε_ℓ^s, is estimated from the Sáez and Carbonell [16] correlation. Accordingly, the dynamic liquid holdup, ε_ℓ^d, is obtained by subtracting the static holdup from the external one. In trickle-bed operation, the catalyst wetting efficiency, η_e, is obtained by solving the phenomenological model of Iliuta et al. [17]. The static, η_s, and dynamic, η_d, components of wetting efficiency are obtained from the Rajashekharam et al. [18] approximation. The liquid-phase axial dispersion coefficients, D_ℓ, and the mass transfer coefficients between dynamic and

Table 1
Parameters used in the simulations

	Fixed beds	Fluidized beds	Slurry-bubble columns
Temperature, °C	80	80	80
Total pressure, MPa	0.5	0.5	0.5
Reactor diameter, cm	5.1	15	15
Bed height, cm	200	200	200
Catalyst particle size, μm	3000	750–1700	200–300
Density of catalyst particle, kg/m^3	1760	1760	1760
Bed porosity, %	36	50–80	
Superficial liquid velocity, m/s	0.0015	0.0035–0.01	0.003–0.006
Superficial gas velocity, m/s	0.028	0.028	0.20
Phenol feed concentration, mol/l	0.001–0.03	0.001	0.001
k_2, mol/kg min	7.6	7.6	7.6
k_2', mol/kg min	53.92	53.92	53.92
k_4, min^{-1}	0.08	0.08	0.08
k_4', min^{-1}	1.92	1.92	1.92
K_1, m^3/mol	0.00124	0.00124	0.00124
K_3, m^3/mol	0.00068	0.00068	0.00068
K_3', m^3/mol	0.0	0.0	0.0

static liquids, $(ka)_{\ell\ell}$, are taken from Ref. [19] for trickle beds and Ref. [20] for packed-bubble columns. The (dynamic) liquid–solid mass transfer coefficient, $k^{\mathrm{d}}_{\ell\mathrm{s}}a_{\mathrm{s}}$, is evaluated as an average from three literature correlations; Refs. [21–23] for trickle beds, and Refs. [24–26] for packed-bubble columns. The (static) liquid–solid mass transfer coefficient, $k^{\mathrm{s}}_{\ell\mathrm{s}}a_{\mathrm{s}}$, is evaluated using Ref. [27]. The effective diffusion coefficients, D_j^{eff}, are evaluated assuming a tortuosity factor equal to 3.

Fluidized bed reactors. The neural network correlations of Larachi et al. [28,29] are used to check for the onset of fluidization, i.e. $v_\ell > v_{\ell\mathrm{mf}}$, and to compute the liquid holdup, ε_ℓ, under the chosen oxidation conditions. The liquid-phase axial dispersion coefficient, D_ℓ, is obtained from the correlation of Kim and Kim [30], and the liquid–solid mass transfer coefficient, $k_{\ell\mathrm{s}}a_{\mathrm{s}}$, from the correlation of Arters and Fan [31].

Slurry-bubble column reactors. The equations of Smith and Ruether [12] are used to determine the solids axial dispersion coefficient, D_{s}, and the hindered settling velocity, v_{p}. The liquid-phase axial dispersion coefficient, D_ℓ, is obtained from the correlation of Kato et al. [11], the gas holdup, ε_{g}, from Ref. [32], and the liquid–solid mass transfer coefficient, $k_{\ell\mathrm{s}}a_{\mathrm{s}}$ from Ref. [33].

2.6. Numerical methods

The partial differential equations for the various reactor models are coupled non-linear equations involving time and space dependencies for each species at the pellet and the reactor scales simultaneously, and are subject to non-homogeneous boundary conditions. Solutions of the above models require a priori knowledge of several hydrodynamic parameters, mass transfer coefficients, and reaction rate expressions. A computer program, using the GEAR method, was developed in Fortran 77, to solve for each reactor and each species in the corresponding system of two-dimensional parabolic partial differential equations. Discretization of the spatial dimension was carried out by the method of orthogonal collocation [34]. The numbers of collocation points specified for the catalyst pellets and reactors are 5 and 9, respectively.

3. Results and discussion

3.1. Trickle bed vs. packed-bubble column

Computing the value of the ratio, γ [35], defined as the ratio of the effective fluxes of both reactants within the particle, scaled by the ratio of stoichiometric

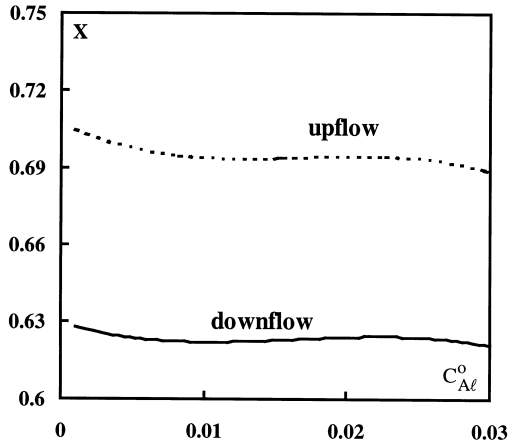

Fig. 2. Phenol conversion vs. inlet phenol concentration — fixed bed reactors ($t = 5$ h).

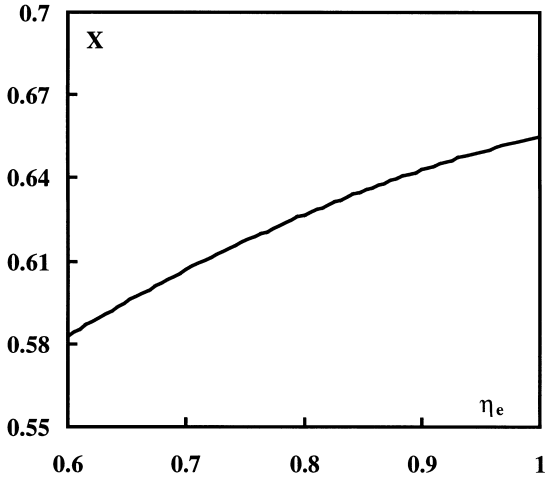

Fig. 3. Phenol conversion vs. external wetting efficiency — trickle bed ($C^{o}_{A\ell} = 0.006$ mol/l, $t = 5$ h).

coefficients, leads to $\gamma < 1$ for the CWO operating conditions simulated in this study. Hence according to the Khadilkar et al. [35] taxonomy, the wet air oxidation is likely to be liquid-reactant limited.

Fig. 2 shows typical phenol overall conversions in cocurrent packed-bubble column and trickle bed for different phenol inlet concentrations after 5 h of operation. The wetting efficiency in trickle bed is ca. 80%, so that the bed does operate with partially wetted pellets. Although under the same tested conditions liquid back-mixing is more prominent in the packed-bubble column than in the trickle bed, the former outperforms the latter, regardless of the feed phenol concentration. Since phenol CWO is liquid-reactant limited, an upflow reactor is preferred as it provides for complete catalyst wetting, and consequently for the fastest transport of liquid reactant to the catalyst. Higher pressure and temperature levels further improve the solubility of oxygen [36] and thus its transfer flux to the pellets. Consequently, the γ-ratio will diminish further under those conditions making upflow operation even more propitious for conducting CWO than a downflow operation. This point may be decisive in the selection, design and scale-up of the three-phase reactor type for hosting the wet oxidation reaction. As catalyst wetting improves, by increasing, e.g. the gas superficial velocity, the difference in the performances by the two modes of reactor operation decreases as shown in Fig. 3 since the trickle-bed pellets become progressively entirely wetted.

Computed reactor profiles of the activity function of the MnO_2/CeO_2 catalyst in the time range [0–200 h] exhibited the expected feature of time-declining activity, especially in the first layers of the bed and in the vicinity of the outer shell of the catalyst surface ($r_p/r > 0.8$) as exemplified in Fig. 4 for the trickle-bed operation. The simulation for the upflow mode, not shown here, follows the same qualitative trend. The autonomy for both reactor configurations would be ca. 10 days before the catalyst becomes severely "coked", after which spent catalyst burn-off and regeneration become important issues for long-term exploitation of the catalyst [37]. It is instructive to learn from these predictions that most of the deactivating carbonaceous material builds up preferentially within a thin peripheral shell, which, as time progresses hampers accessibility for the reactants to the active sites located deep in the catalyst core.

3.2. Fluidized bed and slurry-bubble column

For gas–liquid–solid fluidized-bed reactors, the particle size directly affects their hydrodynamic behavior, and reflects in their phase holdups, solids mixing pattern (no solids mixing or complete solid mixing), mass transfer and chemical reaction rates. Compared with the previous cocurrent packed beds, three-phase

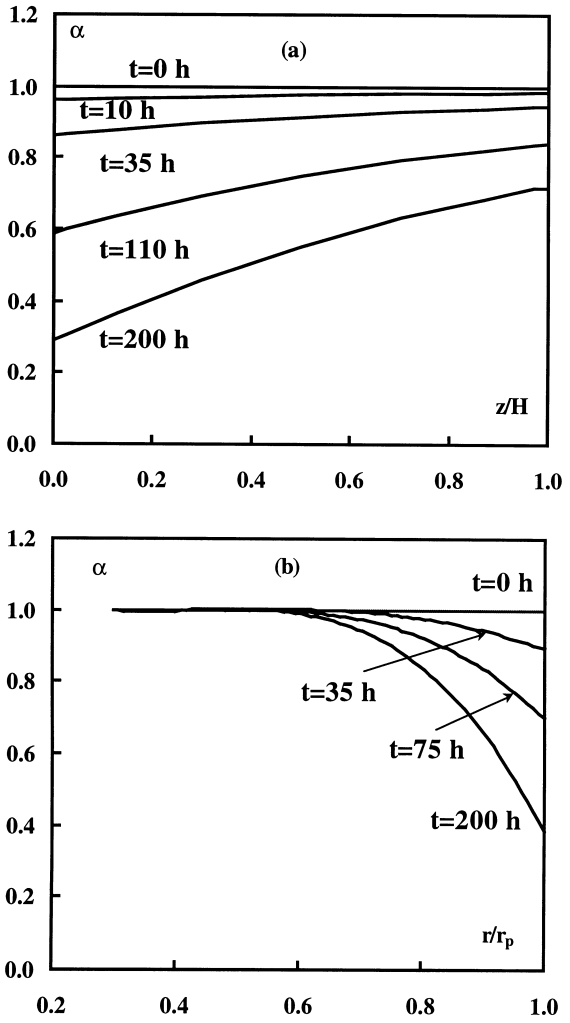

Fig. 4. Variation of the deactivation function with time and (a) dimensionless axial distance for $r/r_p = 0.934$ or (b) with pellet radial distance for $z/H = 0.5$ — trickle bed ($C^o_{A\ell} = 0.006\,\text{mol/l}$).

fluidized beds produce very high back-mixing, especially in the liquid. They are interesting substitutes particularly for adiabatic operation and wastewaters with very high organic loadings. Especially during reactor start-up, shut-down or when sudden changes occur in running conditions, temperature control of the reactor becomes key to prevent the risks of ignition or reactor run-away.

Fig. 5 illustrates the variation with particle diameter of the effectiveness factor and phenol conversion. The simulation, a snapshot at 5 h, is obtained assuming no-solids-mixing pattern for the catalyst (boundary condition given by Eq. (7)). Due to the severe intra-particle mass transfer resistance, the larger the particles, the lower the conversion and the effectiveness factor.

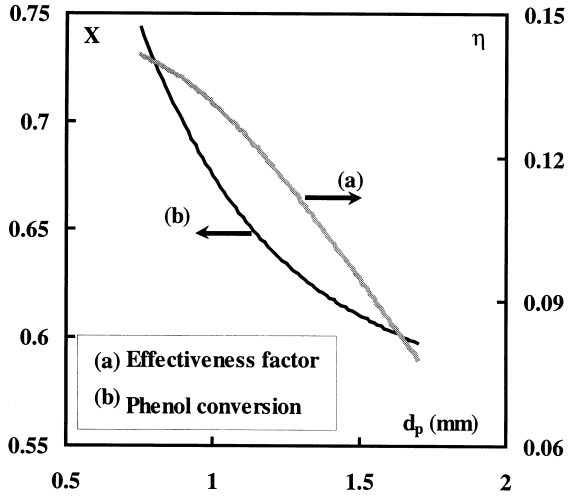

Fig. 5. Variation of the effectiveness factor and phenol conversion vs. particle diameter — fluidized-bed reactor ($C^o_{A\ell} = 0.006\,\text{mol/l}$, $v_\ell = 0.005\,\text{m/s}$, $t = 5\,\text{h}$).

Increasing the liquid superficial velocity lowers the phenol conversion (Fig. 6), presumably because

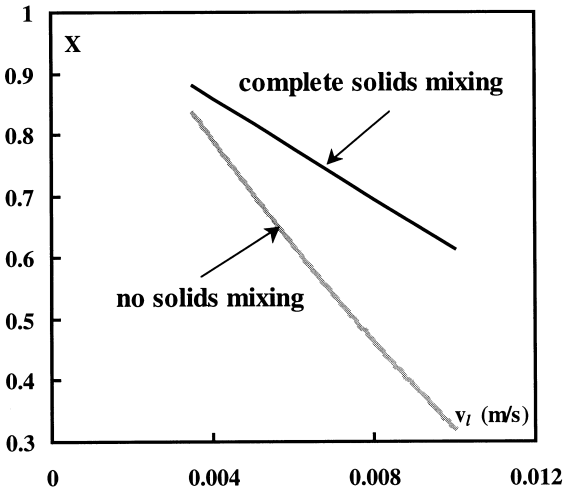

Fig. 6. Phenol conversion vs. superficial liquid velocity in the fluidized bed reactor ($C^o_{A\ell} = 0.006\,\text{mol/l}$, $d_p = 1\,\text{mm}$, $t = 5\,\text{h}$, CSTR: $\eta = 0.116$, plug flow: $\eta = 0.128$).

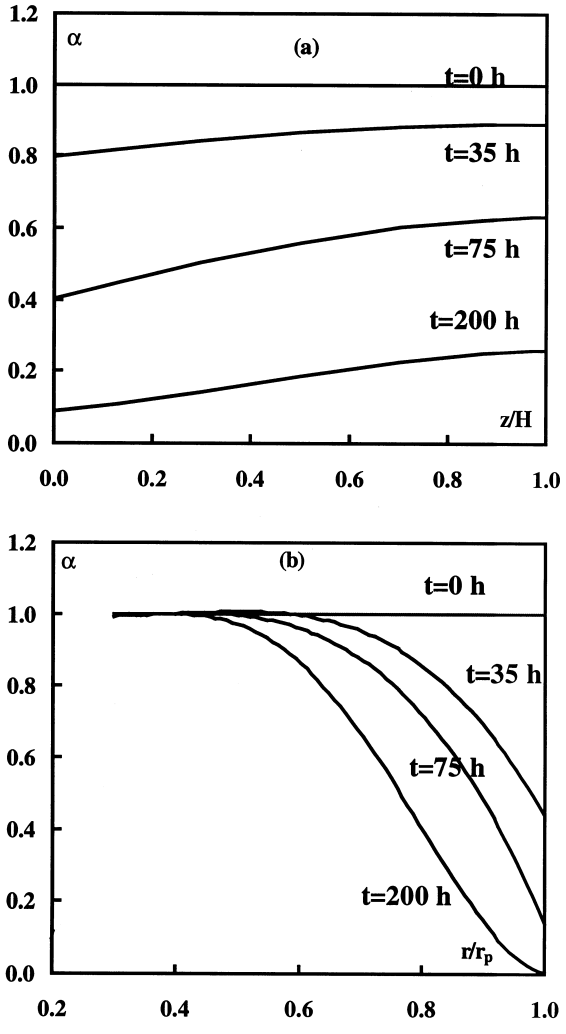

Fig. 7. Variation of the deactivation function with time and (a) dimensionless axial distance for $r/r_p = 0.934$ or (b) with pellet radial distance for $z/H = 0.5$ — fluidized-bed reactor ($C^o_{A\ell} = 0.006\,\text{mol/l}$, $d_p = 1\,\text{mm}$, $v_\ell = 0.005\,\text{m/s}$).

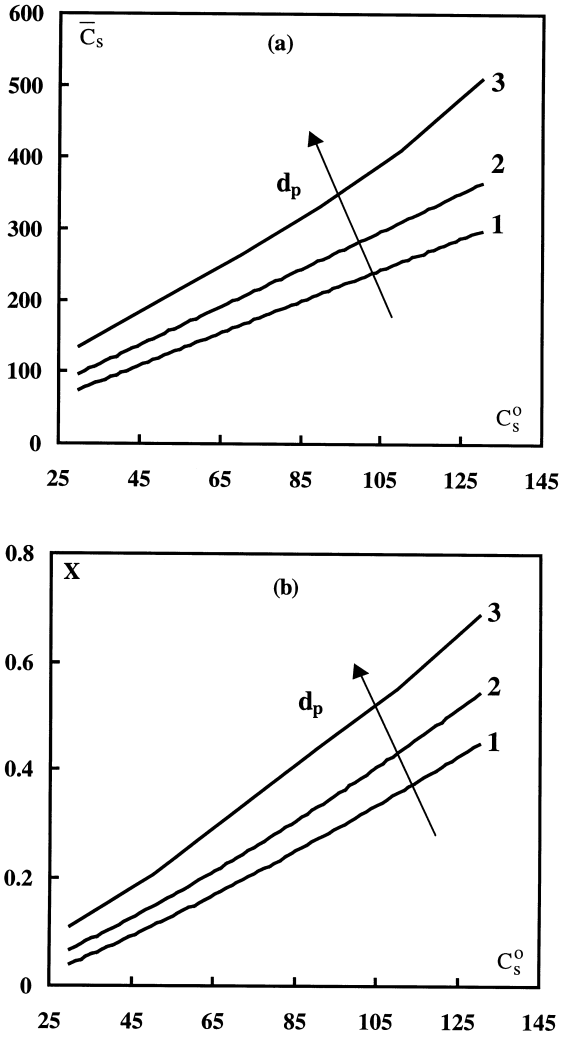

Fig. 8. Influence of solids feed concentration on (a) average solids concentration and (b) phenol conversion in the slurry-bubble column ($C^o_{A\ell} = 0.006\,\text{mol/l}$, $t = 5\,\text{h}$; (1) $d_p = 0.2\,\text{mm}$, (2) $d_p = 0.25\,\text{mm}$, (3) $d_p = 0.3\,\text{mm}$).

of a decrease in solids hold-up (thus in overall reaction rate also) and an increase of liquid back-mixing due to the high liquid and gas superficial velocities [38]. The increased throughput of phenol is another major reason for the drop of the conversion with increasing liquid velocity. Similar deterioration in pollution abatement efficiency, due to an adverse effect of liquid back-mixing, has been also pointed out by Debellefontaine et al. [6] who simulated the dynamics of non-catalytic wet air oxidation for domestic and industrial wastewaters in bubble columns.

Adverse effects of liquid back-mixing on phenol conversion are more dramatic if the catalyst particles evolve in no-solids-mixing pattern rather than exhibiting a complete-solids-mixing pattern (Fig. 6). The difference in reactor performance for these two limiting patterns becomes more serious with increasing liquid superficial velocity, a complete-solids-mixing flow pattern appearing more advantageous the higher

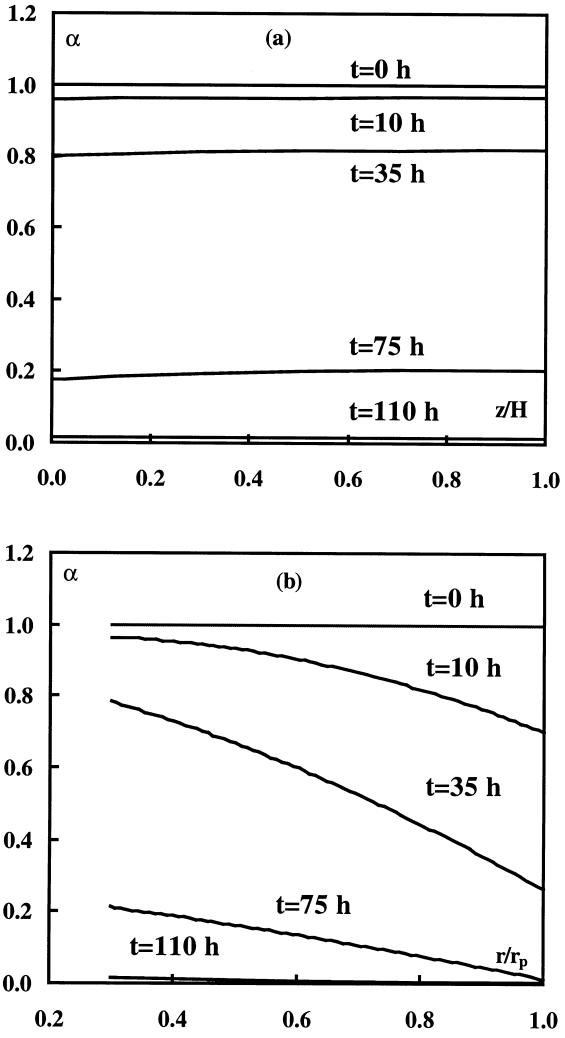

Fig. 9. Variation of the deactivation function with time and (a) dimensionless axial distance for $r/r_p = 0.2975$ or (b) with pellet radial distance for $z/H = 0.5$ — slurry-bubble column ($C^o_{A\ell} = 0.006\,\text{mol/l}$, $d_p = 0.25\,\text{mm}$, $v_\ell = 0.003$ m/s, $C^o_s = 140\,\text{kg/m}^3$).

the liquid throughputs. It is in the bed-bottom region where the reactant-rich pellets contribute most to the conversion, whereas in the upper bed, the catalyst particles are exposed to a liquid with lower phenol concentration. The complete-solids-mixing pattern promotes more frequent intrusions of the pellets in the entrance region which explains the improvements in phenol overall conversion, especially at high liquid superficial velocity.

The computed activity profiles along the reactor longitudinal direction in the time range (0–200 h) exhibited the same qualitative features as in the case of the fixed-bed reactors, see Fig. 7a and b. Here too, especially the outer shell of the catalyst surface ($r_p/r > 0.78$) is most sensitive to deactivation.

Fig. 8a and b shows, respectively, the evolution of average solids concentration and phenol overall conversion in the slurry as a function of the catalyst powder size and feed concentration. Phenol conversion increases both with increasing catalyst size and with increasing feed solids concentration. Apparently the increased liquid–solid contacting area with the increased powder size largely offsets the corresponding reduction in effectiveness factor with increasing sizes ($\eta = 0.376$ for $d_p = 0.3\,\text{mm}$; $\eta = 0.45$ for $d_p = 0.25\,\text{mm}$ and $\eta = 0.549$ for $d_p = 0.2\,\text{mm}$), see Fig. 8b. The activity decline along the reactor stream-wise coordinate and across the catalyst particles is illustrated in Fig. 9a and b which shows virtually quasi-death of the catalyst after 110 h of operation. Due to its smaller size, the activity loss affects the whole bulk of the catalyst particle.

Comparison of the overall phenol conversion in fluidized bed and slurry-bubble column having the same diameter and height and subject to the same waste-

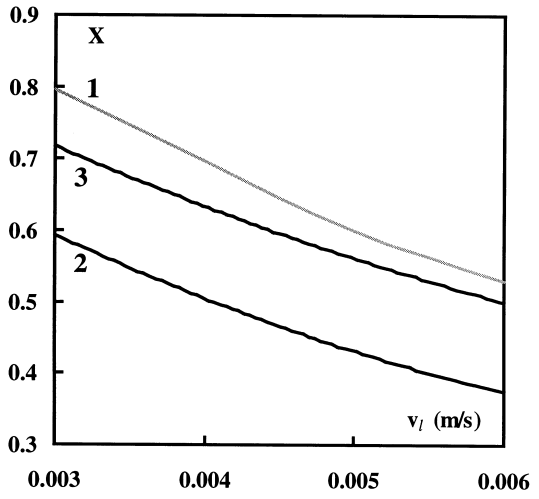

Fig. 10. Phenol conversion vs. v_ℓ ($v_g = 0.2\,\text{m/s}$, $C^o_{A\ell} = 0.006\,\text{mol/l}$, $d_p = 1\,\text{mm}$ fluidized bed; $d_p = 0.25\,\text{mm}$ slurry, $t = 5\,\text{h}$). Fluidized bed reactor (curve 1); slurry-bubble column: curve 2 for $C^o_s = 110\,\text{kg/m}^3$; curve 3 for $C^o_s = 140\,\text{kg/m}^3$.

water effluent indicates that for the simulation conditions of Table 1, three-phase fluidization is a better option than slurry-bubble columns (Fig. 10). The higher solids holdup in the former could be a valid explanation of this observation as confirmed by the closeness of performances of the fluidized bed and the slurry reactor with the higher catalyst concentration in the feed (curve 3 in Fig. 10).

4. Closing remarks

Compared to other mature industrial sectors where multiphase reactor technology is routine, the design of three-phase catalytic reactors for wet air oxidation processes is still at an emerging stage. So far, commercial-scale plants applying solid-catalyzed wet oxidation for the removal of organic pollution from industrial or domestic wastewater are rare [5]. Despite an explosion in recent years of academic and patent literature with studies on intrinsic kinetics and solid catalyst optimization for heterogeneously catalyzed wet oxidation, so far only timid progress has been achieved on the reactor engineering front. Since the design of such three-phase reactors is a complex task due to the demanding levels of temperature and pressure, and due to the complex intermingling between hydrodynamics, flow patterns, thermodynamics, and macro-/micro-kinetic phenomena, there is an urgent need to bring new knowledge and information from the perspective of multiphase reactor engineering.

This study, although purely theoretical in nature, is the first of its kind to address the question of catalyst deactivation in catalytic wet oxidation for four of the most common three-phase catalytic reactors, i.e. trickle-beds, packed-bubble columns, three-phase fluidized beds and slurry-bubble columns.

The goal was not to come to sharp conclusions regarding which reactor is the best suited for catalytic wet oxidation. Rather, this study attempts to set the wet oxidation reactor modeling by integrating the most pertinent features of the molecular, particle and reactor scales to discuss the interplay between reaction kinetics, transport phenomena and hydrodynamics. These preliminary results suggest that liquid-reactant limited reactions such as wet oxidation are better performed in packed-bubble columns rather than trickle beds, and that slurry-bubble columns are most vulnerable to "coke" deactivation.

References

[1] R.A. Sheldon, J. Chem. Technol. Biotechnol. 68 (1997) 381.
[2] P.L. Mills, R.V. Chaudhari, Catal. Today 48 (1999) 17.
[3] F.J. Zimmerman, D.G. Diddams, TAPPI 43 (1960) 710.
[4] Y.I. Matatov-Meytal, M. Sheintuch, Ind. Eng. Chem. Res. 37 (1998) 309.
[5] F. Luck, Catal. Today 53 (1999) 81.
[6] H. Debellefontaine, S. Crispel, P. Reilhac, F. Périé, J.-N. Foussard, Chem. Eng. Sci. 54 (1999) 4953.
[7] S. Schlüter, A. Steiff, P.M. Weinspach, Chem. Eng. Process. 31 (1992) 97.
[8] S. Hamoudi, K. Belkacemi, F. Larachi, Chem. Eng. Sci. 54 (1999) 3569.
[9] S. Hamoudi, F. Larachi, A. Adnot, A. Sayari, J. Catal. 185 (1999) 333.
[10] A. Pintar, J. Levec, J. Catal. 135 (1992) 345.
[11] Y. Kato, A. Nishiwaki, T. Fukuda, S. Tanaka, J. Chem. Eng. Jpn. 5 (1972) 112.
[12] D.N. Smith, J.A. Ruether, Chem. Eng. Sci. 40 (1985) 741.
[13] W. O'Dowd, D.N. Smith, J.A. Ruether, S.C. Saxena, AIChE J. 33 (1987) 1959.
[14] I. Iliuta, F. Larachi, B.P.A. Grandjean, Ind. Eng. Chem. Res. 37 (1998) 4542.
[15] Z. Bensetiti, F. Larachi, B.P.A. Grandjean, G. Wild, Chem. Eng. Sci. 52 (1997) 4239.
[16] A.E. Sáez, R.G. Carbonell, AIChE J. 31 (1985) 52.
[17] I. Iliuta, F. Larachi, B.P.A. Grandjean, Chem. Eng. Res. Design 77 (1999) 759.
[18] M.V. Rajashekharam, R. Jaganathan, V. Chaudhari, Chem. Eng. Sci. 53 (1998) 787.
[19] I. Iliuta, F.C. Thyrion, O. Muntean, Can. J. Chem. Eng. 74 (1996) 783.
[20] I. Iliuta, F.C. Thyrion, O. Muntean, M. Giot, Chem. Eng. Sci. 51 (1996) 4579.
[21] V. Specchia, G. Baldi, A. Gianetto, in: Proceedings of the Fourth International/Sixth European Symposium on Chem. React. Eng., Vol. 7, 1976, p. 390.
[22] S. Goto, J.M. Smith, AIChE J. 21 (1975) 706.
[23] C.N. Satterfield, M.W. van Eek, G.S. Bliss, AIChE J. 24 (1978) 709.
[24] V. Specchia, G. Baldi, A. Gianetto, Ind. Eng. Chem. Process. Des. Dev. 17 (1978) 362.
[25] S. Mochizuki, T. Matsui, Chem. Eng. Sci. 29 (1974) 1328.
[26] G. Delaunay, A. Storck, A. Laurent, J.C. Charpentier, Ind. Eng. Chem. Process. Des. Dev. 19 (1980) 514.
[27] I. Iliuta, F. Larachi, B.P.A. Grandjean, Chem. Eng. Sci. 54 (1999) 4099.
[28] F. Larachi, I. Iliuta, O. Rival, B.P.A. Grandjean, Ind. Eng. Chem. Res. 39 (2000) 563.
[29] F. Larachi, L. Belfares, I. Iliuta, B.P.A. Grandjean, 2000, I&EC Res., submitted.

[30] S.D. Kim, C.H. Kim, J. Chem. Eng. Jpn. 16 (1983) 172.
[31] D.C. Arters, L.S. Fan, Chem. Eng. Sci. 41 (1986) 107.
[32] W.D. Deckwer, Bubble Column Reactors, Wiley, New York, 1992.
[33] P. Sanger, W.D. Deckwer, Chem. Eng. J. 22 (1981) 179.
[34] B.A. Finlayson, The Method of Weighted Residuals and Variational Principles, Academic Press, New York, 1972.
[35] M.R. Khadilkar, Y.X. Wu, M.H. Al-Dahhan, M.P. Dudukovic', M. Colakyan, Chem. Eng. Sci. 51 (1996) 2139.
[36] D.M. Himmelblau, J. Chem. Eng. Data 5 (1960) 10.
[37] F. Larachi, K. Belkacemi, S. Hamoudi, A. Sayari, 2000, Catal. Today, in press.
[38] L.S. Fan, Gas–Liquid–Solid Fluidization Engineering, Butterworths Series in Chemical Engineering, Butterworths, London, 1989.